Aug 20th, 12:00 AM

Impact Loading of Thin-walled Beams

Edward A. Zanoni

Charles G. Culver

IMPACT LOADING OF THIN-WALLED BEAMS

By Edward A. Zanoni[1] and Charles G. Culver,[2] Assoc. Members, ASCE

INTRODUCTION

The behavior of individual thin compression elements subjected to a time varying load applied in the middle plane was discussed in a previous paper (2)[3]. The purpose of this paper is to present an analytical method for determining the dynamic response of thin-walled flexural members subjected to short duration impact loading. Results obtained from this mathematical model are compared with experimental values obtained from beams subjected to impact loading.

BEHAVIOR OF THIN-WALLED BEAMS

For illustrative purposes in this paper, the thin-walled beam with a "hat" shaped cross section shown in Fig. 1 will be considered. Note, however, that the general mathematical method described herein is also applicable to any thin-walled beam with singly symmetric cross section loaded in the plane of symmetry.

The sign convention used for positive bending moment is shown at the top of Fig. 1. In the following, the term "as built" will be used when referring to the cross sectional properties (moment of inertia, section modulus, etc.) of this initial unstressed cross section. When the compressive bending stresses reach a certain value, the plate element comprising the top flange of the cross section buckles and the concept of "effective width" is used to evaluate the properties of the buckled cross section. Referring to Fig. 1, the cross sectional dimensions such as w and f, referred to as "flat widths" are used to establish the stress level at which this buckling occurs.

For the specific cross section in Fig. 1, it will be assumed that only a positive bending moment will cause buckling; i.e., the f/h ratio is so small [$(f/h) < (w/h)_{lim}$ ... Ref. 9] that any compressive bending stress in the bottom flange due to a negative bending moment will not exceed the buckling stress σ_{cr}. An empirical formulation of σ_{cr} is available:

$$\sigma_{cr} = \frac{(1.6556)\,E}{(w/h)^2} \qquad \ldots\ldots (1)$$

Eq. 1 is usually expressed in the form of a limiting width-to-thickness ratio, $(w/h)_{lim}$, below which the plate will not buckle.

Above this stress level, an effective width, b, must be calculated according to the following formula:

$$b = 1.9\,h\sqrt{\frac{E}{\bar{\sigma}_{max}}}\left[1.0 - 0.415(h/w)\sqrt{\frac{E}{\bar{\sigma}_{max}}}\right] \qquad \ldots (2)$$

In Eqs. 1, 2, all dimensions are in inches and the stress and modulus of elasticity are in ksi. Substituting $E = 29.5 \times 10^3$ ksi. and $\bar{\sigma}_{max} = 1.67\sigma$, 1.67 being the factor of safety, in Eq. 2 gives the formula for the effective design width of stiffened compression elements in the current specification (9). Thus two distinct stress conditions are possible, depending on the magnitude of the moment as noted at the bottom of Fig. 1. Computation of the section properties using Eqs. 1,2 requires some iteration since the actual stress must reflect the reduced cross sectional properties (12).

If the same type of cross section is used often enough, it may be desirable to develop nondimensional curves for the section properties as shown in Fig. 2. In plotting these curves, the as built cross sectional properties, I_o, S_{TO}, S_{BO}, were used as reference values. The reduction in the cross sec-

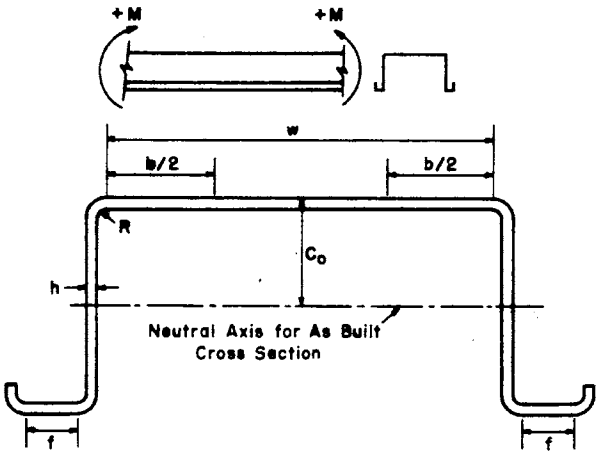

I_o = "As built" moment of inertia

M_{LB} = "Local buckling" moment

σ_T = Maximum top flange bending stress

σ_{cr} = Stress at which local buckling first occurs

$\sigma_{cr} = (1.6556\,E)/(w/h)^2$

If $\sigma_T \le \sigma_{cr}$:	If $\sigma_T > \sigma_{cr}$:
$\sigma_T = Mc/I$	$\sigma_T = Mc/I$
$b = w$	$b = 1.9h\sqrt{E/\sigma_T}\left[1.0 - 0.415(h/w)\sqrt{E/\sigma_T}\right]$
$I = I_o$	$b \neq w$; $I < I_o$
$c = c_o$	$c > c_o$

$M_{LB} = \sigma_{cr} I_o / c_o$

FIG. 1 - Typical Light Gage Cross Section

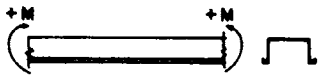

As built properties:

I_o = Moment of Inertia

S_{TO} = Section modulus.. top flange

S_{BO} = Section modulus.. bottom flange

M_{LB} = Local buckling moment = $\sigma_{cr} S_{TO}$

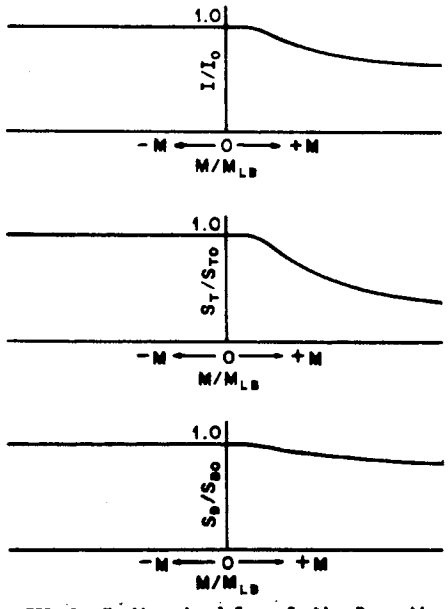

FIG. 2 - Nondimensional Cross Section Properties

[1]Senior Engr., Bettis Atomic Div., Westinghouse Electric Corp., Pittsburgh, Pa.

[2]Assoc. Prof. of Civ. Engrg., Carnegie-Mellon University, Pittsburgh, Pa.

[3]Numerals in parentheses refer to corresponding items in Appendix I - References

tional properties as the stress level increases above σ_{cr}, $M^+ > M_{LB}$, is apparent. Since the flat width ratio for the bottom flange elements was assumed to be small such that these elements do not buckle, the cross sectional properties of the beam subjected to negative bending are the same as the as built properties, $M/M_{LB} < 0$, $I/I_o = 1$, etc. Note that despite that fact that the cross section buckles, the stress levels in the range where $\sigma_T > \sigma_{cr}$ are within the elastic range of the material and yielding does not commence until the internal moments exceed the values indicated by the termination of the curves in Fig. 2. Since only a limited amount of rotation capacity is available after initial yield, the present specification for cold-formed beams does not take into account any redistribution of moments or plastic design. The analysis presented herein is also limited to the elastic range of the material, $\bar{\sigma}_{max} \leq \sigma_y$.

As noted previously, the relationship for σ_{cr} presented in Ref. 9 and Eq. 1 is based on extensive static tests (11). However, a recent analytical study (2) indicated that the time duration of the stress level may be an important factor when considering the dynamic response of thin plates. Direct application of these results to beam response, however, would be difficult and was not considered in the development of the mathematical model herein. The concept of a dynamic effective width will be considered, however, in evaluating the test results.

MATHEMATICAL MODEL

Consider the simply supported beam in Fig. 3a subjected to a system of external forces P_i. The continuous system is idealized by a series of lumped masses connected by flexible elements. This idealization is advantageous since the resulting mathematical model consists of a system of simultaneous ordinary differential equations rather than a partial differential equation. Neglecting damping, the equations of motion of the system of mass points can be written in matrix form as:

$$\left[m_i \right] \left\{ \ddot{y}_i \right\} + \left[A \right]_B^{-1} \left\{ y_i \right\} = \left\{ P_i \right\} \quad . \quad . \quad . \quad (3)$$

For a linear elastic system, the matrix $\left[A \right]_B$, referred to as the beam flexibility matrix, remains constant with time.

The basic difficulty with using Eq. 3 for thin-walled members subject to dynamic loading is that the flexibility matrix becomes time dependent and is continously changing since the moment of inertia changes with the stress level. This difficulty was overcome by using an incremental form of solution. For each small time increment, it was assumed that the stiffness characteristics of the beam could be represented by stationary nonlinear relationships of the form shown in Fig. 2. For a particular time increment the beam flexibility matrix was assumed to remain constant and was evaluated using the distribution of moments from the preceding time step.

Since the moment of inertia varies along the beam according to the stress level, the beam is a nonprismatic structure. The beam flexibility matrix $\left[A \right]_B$ was therefore computed by subdividing the portions of the beam between the lumped masses in Fig. 3a into a series of flexible elements. The moment of inertia was assumed to vary linearly over the length of each element. Treating an individual element as a cantilever beam, assuming the moment of inertia at the free end x = 0, I(0), is larger than that at the fixed end, I(ℓ), and using the principle of virtual work (1), the flexibility coeffieients for deflection and rotation due to a shear force V_e and moment M_e applied at the free end become:

$$\begin{Bmatrix} \delta_v \\ \delta_M \end{Bmatrix} = \begin{bmatrix} a_{11} & a_{12} \\ a_{21} & a_{22} \end{bmatrix} \begin{Bmatrix} V_e \\ M_e \end{Bmatrix} \quad . \quad . \quad . \quad . \quad (4)$$

where:

$$a_{11} = (1/E)\int_0^{\ell} \left[x^2/(I(0) - mx) \right] dx \quad . \quad . \quad . \quad . \quad (5a)$$

$$a_{12} = a_{21} = (1/E)\int_0^{\ell} \left[x/(I(0) - mx) \right] dx \quad . \quad . \quad . \quad . \quad (5b)$$

$$a_{22} = (1/E)\int_0^{\ell} \left[1/(I(0) - mx) \right] dx \quad . \quad . \quad . \quad . \quad (5c)$$

$$m = \left[I(0) - I(\ell) \right]/\ell \quad . \quad . \quad . \quad . \quad . \quad . \quad . \quad (5d)$$

Note that shearing deflections were neglected in establishing Eqs. 5. Similar expressions may be obtained for the case in which I(ℓ) > I(0) by redefining m. In general Eq. 4 may be written as:

$$\begin{Bmatrix} \delta_v \\ \delta_M \end{Bmatrix}_e = \left[A \right]_e \begin{Bmatrix} V \\ M \end{Bmatrix}_e \quad . \quad . \quad . \quad . \quad . \quad . \quad (6)$$

where the subscript e is used to denote element and the element flexibility matrix is denoted as $\left[A \right]_e$. The flexibility matrix for the entire beam is then computed in the following manner. By definition:

$$\left\{ \delta_i \right\} = \left[A \right]_B \left\{ P_i \right\} \quad . \quad . \quad . \quad . \quad . \quad . \quad . \quad (7)$$

where

P_i = applied loads on the beam

δ_i = working deflections of P_i

$\left[A \right]_B$ = beam flexibility matrix

The moment and shear at the end of each beam element can be expressed as:

$$\begin{Bmatrix} V \\ M \end{Bmatrix}_e = \left[C \right]_e \left\{ P_i \right\} \quad . \quad . \quad . \quad . \quad . \quad . \quad . \quad (8)$$

The matrix $\left[C \right]_e$ is determined from static equilibrium principles. The beam flexibility matrix is finally computed as:

$$\left[A \right]_B = \sum_{e=1}^{j} \left(\left[C \right]^T \left[A \right] \left[C \right] \right)_e \quad . \quad . \quad . \quad . \quad . \quad . \quad (9)$$

where the beam is made up of j elements. The above procedure may be applied to the idealized lumped mass beam shown in Fig. 3a. As indicated in Fig. 3b, variable element lengths $\lambda_1 L$, $\lambda_2 L$, ...etc. may be used between the discrete mass points. This variation is permitted in the event that it is necessary to have more elements in one location of the model than another. For example, in regions where steep stress gradients are expected, more elements may be required than in regions where the stress is expected to be more uniform. If the moment of inertia at the ends of the elements, as well as the element length, are expressed in nondimensional form as I/I_o and λ respectively, and the element flexibility coefficients as well as the matrix $\left[C \right]_e$ are evaluated accordingly, Eq. 9 will not yield $\left[A \right]_B$ but a nondimensional matrix $\left[F \right]_B$. However, the properties of this matrix are such that the following relationship is true:

$$(L^3/EI_o) \left[F \right]_B = \left[A \right]_B \quad . \quad . \quad . \quad . \quad . \quad . \quad (10)$$

Nondimensional Equations for Lumped Mass Model

In order to illustrate the influence of the significant parameters governing the dynamic response, it is advantageous to nondimensionalize Eq. 3. For example, any load pulse acting at the mass points can be defined as a function of a characteristic magnitude. That is, the dimension of force may be factored out so that each load pulse is represented by a common load factor multiplied by the appropriate time varying coefficient. An example of a characteristic load pulse is shown in Fig. 3c. The characteristics of the pulse are the magnitude P_m, and the duration t_d. In the following development the forcing functions acting on the lumped mass model will always be expressed in this form. Also, since the lumped masses m_i represent some fraction of the total beam mass M, the diagonal mass matrix has a common factor. Considering Eq. 10, the following relationships are obtained:

$$\left[m_i \right] = (M) \left[b_i \right] \quad . \quad . \quad . \quad . \quad . \quad . \quad (11a)$$

$$\left[A \right]_B^{-1} = (EI_o/L^3) \left[F \right]_B^{-1} \quad . \quad . \quad . \quad . \quad . \quad (11b)$$

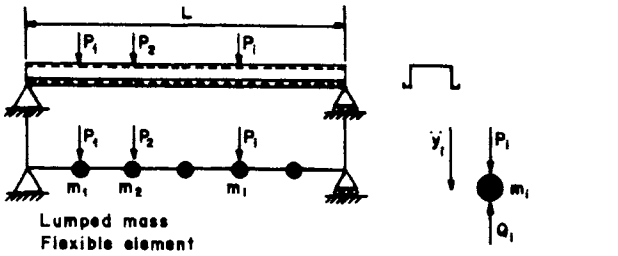

a. Lumped Mass Idealization Of Beam

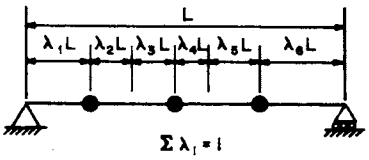

b. Beam Having Elements Of Varible Length

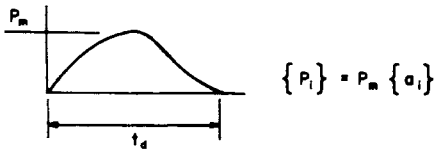

c. Characteristic Load Pulse

FIG. 3 - Typical Lumped Mass Models

$$\{P_i\} = (P_m)\{a_i\} \quad . \quad . \quad . \quad . \quad . \quad . \quad . \quad (11c)$$

Substituting Eqs. 11 into Eq. 3 and rearranging terms gives:

$$\{\ddot{y}_i\} = (P_m/M)[b_i]^{-1}\{a_i\} - (EI_o)/(ML^3)[b_i]^{-1}[F]_B^{-1}\{y_i\} \quad . \quad . \quad (12)$$

Since shearing deflections were neglected, a characteristic deflection δ_p may be defined as:

$$\delta_p = (P_m L^3)/(\eta EI_o) \quad . \quad . \quad . \quad . \quad . \quad . \quad . \quad (13)$$

A pseudo fundamental natural period of the beam, t_o, based on the as built properties is defined as:

$$t_o = (2/\pi)\sqrt{(ML^3)/(EI_o)} \quad . \quad . \quad . \quad . \quad . \quad . \quad (14)$$

Introducing the following nondimensional parameters:

$$x_i = y_i/\delta_p \quad . \quad . \quad . \quad . \quad . \quad . \quad . \quad (15a)$$

$$\tau = t/t_d \quad . \quad . \quad . \quad . \quad . \quad . \quad . \quad . \quad (15b)$$

$$d^2x_i/d\tau^2 = \ddot{x}_i = (t_d^2/\delta_p)(d^2y_i/dt^2) = (t_d^2/\delta_p)\ddot{y}_i \quad . \quad . \quad . \quad . \quad (15c)$$

expressing the time coefficients a_i in nondimensional form a_i',[$a_i = f(t/t_d)$], and using Eqs. 13, 14, Eq. 12 becomes:

$$\{\ddot{x}_i\} = [C_1\beta^2][a_i'/b_i] - [C_2\beta^2][b_i]^{-1}[F]_B^{-1}\{x_i\} \quad . \quad . \quad . \quad (16)$$

where

$$C_2 = 4/\pi^2 \; ; \; C_1 = \eta C_2 \quad . \quad . \quad . \quad . \quad . \quad . \quad (17)$$

The internal moment M_e acting at any element along the beam can also be nondimensionalized. This moment can be expressed as:

$$M_e = (L)[CR]_e\{Q_i\} \quad . \quad . \quad . \quad . \quad . \quad . \quad (18)$$

where the matrix $[CR]_e$ is determined on the basis of the nondimensional element lengths λ. Noting that the net force Q_i acting at a mass point is the difference between the external force P_i and the inertia force, Eq. 18 becomes:

$$(M_e/P_mL) = [CR]_e\left\{a_i' - (b_i\ddot{x}_i)/(C_1\beta^2)\right\} \quad . \quad . \quad . \quad . \quad (19)$$

Since the nonlinearity of the beam was expressed in nondimensional form in terms of I/I_o vs M/M_{LB}, Fig. 2, the moment M_e will be nondimensionalized with respect to M_{LB}. Introducing the parameter $\alpha = M_c/M_{LB}$ where M_c is some characteristic moment of the beam given by:

$$M_c = P_mL/\xi \quad . \quad . \quad . \quad . \quad . \quad . \quad . \quad . \quad (20)$$

Eq. 19 becomes:

$$(M_e/M_{LB}) = (\xi\alpha)[CR]_e\left\{a_i' - (b_i\ddot{x}_i)/(C_1\beta^2)\right\} \quad (21)$$

Note that the coefficient ξ is introduced only as a matter of convenience so that the characteristic moment M_c can be specified as any fraction of a maximum static moment. The calculation of M_e/M_{LB} is not affected by the choice of this parameter.

The equations of motion, Eq. 16, were solved by a numerical integration technique developed by Newmark (5) using the assumption that the accellerations vary linearly within each time increment. Instead of an iterative type solution, appropriate recurrence relationships were employed (10). The number of lumped masses used to idealize the beam and the size of the time increment required to obtain the desired degree of accuracy were determined (5) from comparisons with existing solutions. A seven mass model and a time increment equal to 10% of the lowest natural period of the system (13) were found to yield excellent results. Note that the time increment used remained constant throughout a particular dynamic response calculation. These equations were solved using a computer program written in FORTRAN V for a UNIVAC 1108 digital computer. In addition to the digital output from this program, a plotting routine available with the computer was employed to obtain a graphical presentation of the time variation of the stresses and deflections for each problem. A listing of this program and the complete mathematical development of the equations presented herein is available elsewhere (13).

EXPERIMENTAL PROGRAM

In order to check the mathematical model, a series of static and dynamic beam tests were conducted. A total of eight beams cold-formed from sheet material (AISI HR-1008) using the press-brake method were tested. The virgin sheet material had a sharp yielding type stress strain behavior. Two different values were selected for the flat width ratios of the compression flange of the specimens (Group A, Group B). These values were well above the limiting ratio, $(w/h)_{lim.}$, in order to insure that the dynamic response of the beams would be in the postbuckling or nonlinear elastic range.

The nominal as ordered dimensions of the specimens are shown in Fig. 4a. Average values of the cross sectional dimensions obtained from measurements at five locations along the span length of each beam were used for calculation purposes. The mechanical properties of the specimens were determined from tension and compression coupons cut from extra lengths of the fabricated beams as shown in Fig. 4b.

Static Tests

Four of the eight specimens, two from each group, were tested statically to determine the relationship between the applied moment and the section properties, Fig. 2. The setup and instrumentation for these tests was similar to that employed in previous studies (3). Solid plate web stiffeners of the same thickness as the beams were used at the load points and end supports. In order to insure that the buckling pattern of the compression flange was not inhibited by any local restraint, the stiffeners were cut short of the compression flange and tack welded to the webs. Both positive and negative moment tests were conducted for each group of specimens.

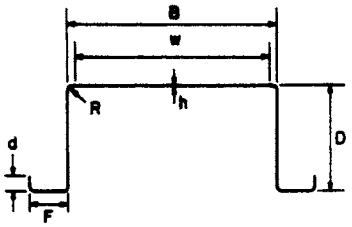

Specimen	B	D	F	d	R	h	w	w/h
A	8	4	1.5	0.5	3/32	0.06	7.69	128.21
B	5 3/4	4	1.5	0.5	3/32	0.06	5.44	90.21

All dimensions are given in inches.

a. Cross sectional properties of beams as ordered.

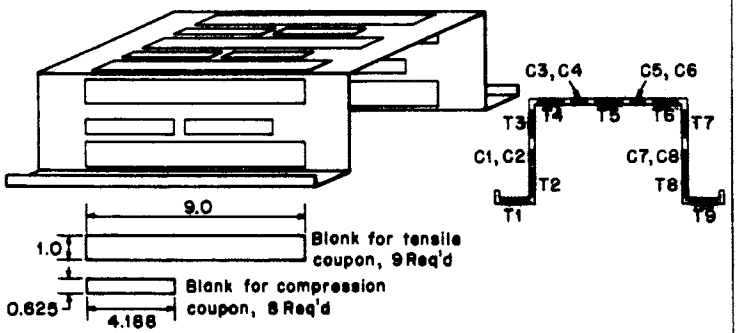

b. Location of tension and compression coupons.

FIG. 4 - Dimensions of Test Specimens

All the strain gages, SR-4 Type A1, were located at the center of the test span and were read individually. Mid plane strains were determined by averaging the two gage readings at each location. Dial gages were located on both sides of the cross section at intervals in the constant moment region. These gages as well as those at the end supports were used to determine the beam deflections. The strain gages and dial gages permitted an evaluation of any tending of the beam to twist under load.

A 60 Kip Baldwin hydraulic testing machine was used for the static tests. Load was applied in small increments, approximately 500 lbs., and sufficient time was taken to allow the strain gages to stabilize before readings were recorded. Near ultimate, increments of deflection rather than load were used and the dial gage readings were stabilized before recording the data. Visual observation of local buckling and yielding was facilitated by whitewashing the specimens.

The data from the tensile and compressive coupons indicated that the yield stress and modulus of elasticity did not vary significantly over the beam cross section due to cold working effects (less than 2% variation). Values for the modulus of elasticity and yield stress for the Group B specimens were, however, lower than expected for the sheet material used. The tensile and compressive yield stresses were also approximately the same (within 3%). These properties did vary between the two groups of specimens, A and B, and it was apparent that different virgin sheet material had been used to fabricate each group. For calculation purposes, the following average values were used: Group A - $E = 29.5 \times 10^3$ ksi., $\sigma_y = 31.2$ ksi; Group B - $E = 27.0 \times 10^3$ ksi., $\sigma_y = 28.7$ ksi.

Typical results from the static beam tests are shown in Fig. 5. Using the strain gage readings to determine the location of the neutral axis and equilibrium considerations for the cross section under pure bending (11), the effective width, internal resisting moment and effective moment of inertia were determined for each value of the external load. Since there was a slight amount of twisting of the specimens, as indicated by the dial gages and strain gages, the calculated internal moment differed slightly (less than 5 %) from the external moment computed from the testing machine load. This unavoidable twisting did not significantly affect the effective width determination, however. The moment indicated for the test points corresponds to the internal moment based on the calculations using the strain gage data.

For comparison purposes the calculated moment of inertia based on Eq. 2 and the average mechanical properties is also shown in Fig. 5. As shown, the section was slightly stiffer than indicated by Eq. 2. As the moment increased, however, the test values approached those determined from Eq. 2. Since negative moment did not produce local buckling, no reduction in the moment of inertia occurred as indicated. The same general trend shown in Fig. 5 was observed for the specimens in group B.

The load deflection curve for the beams subjected to positive moment was nonlinear (3) due to local buckling effects. Attempts were made to determine whether this curve had a horizontal plateau or if any rotation capacity was available similar to that of the heavier hot rolled wide flange shapes. No rotation capacity was present and the load deflection curve began to decrease and the section unloaded after reaching a load approximately 6% higher than the load at which initial yielding of the beam was indicated by the strain gages.

Dynamic Tests

Two loading conditions were used for the dynamic tests, centerline loading and quarter point loading. For quarter point loading, a considerably longer length of the beam was subjected to moment greater than the local

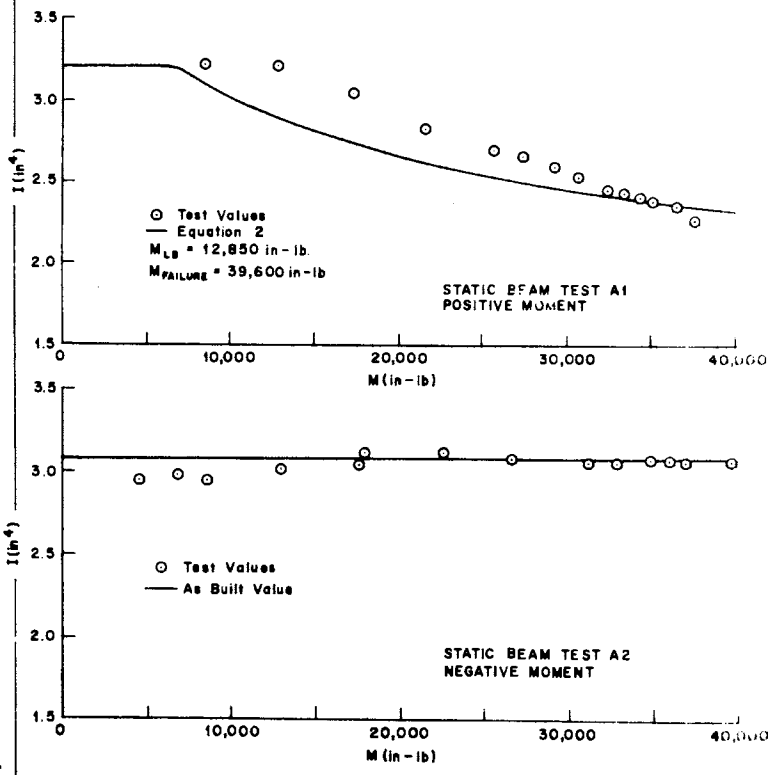

FIG. 5 - Moment of Inertia vs. Moment - Experimental

buckling moment than in the centerline loading case. A sketch of the dynamic test setup for centerline loading is shown in Fig. 6.

The dynamic loads for these tests were developed by dropping a cali-

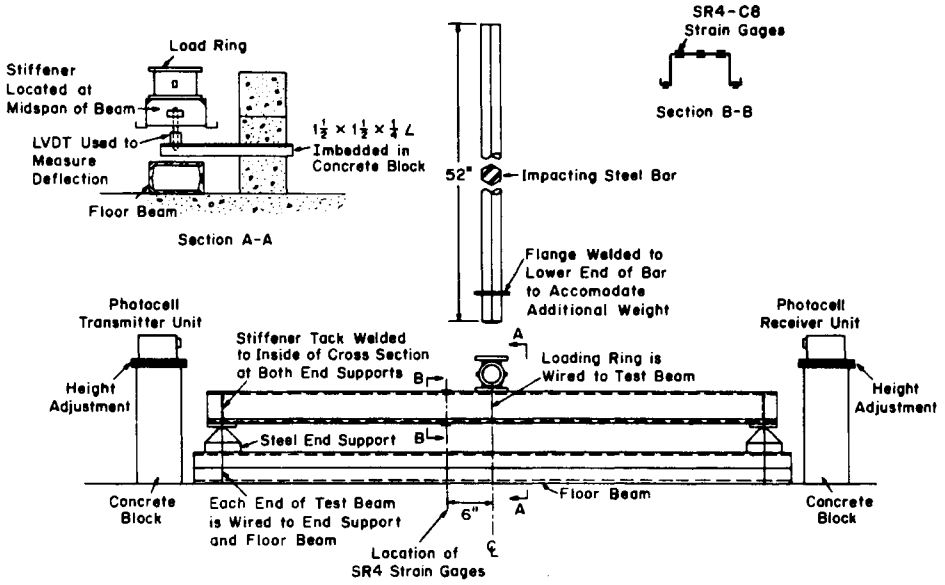

FIG. 6 - Typical Dynamic Beam Test Setup - Mid Span Loading

brated weight from a predetermined height on a load ring attached to the beam. After impact, the weight was immediately removed and the beam was permitted to vibrate freely. For quarterpoint loading, two load rings and a spreader beam were employed. The magnitude and time variation of the applied loads were obtained from photographic records of the oscilloscope traces produced by the strain gages attached to the loading rings. Dynamic strains in the beam were recorded in the same manner. All the strain gages used in the dynamic tests were SR-4 Type C8 dynamic gages. Dynamic deflections were measured by means of a linear variable differential transformer. The photocells shown in Fig. 6 were used to actuate the electric recording circuit as the weight struck the loading ring or spreader beam. Complete details of the test setup and test procedure are available elsewhere (13).

Typical dynamic test results are shown for centerline loading in Fig. 7 and quarterpoint loading in Fig. 9. The midplane stresses at the middle and edge of the compression flange, the midplane stress in the tension flange, the centerline deflection and the variation of the load as recorded by the loading rings are shown. There figures were obtained by enlarging and tracing photographs of the oscilloscope records. Stresses were obtained by multiplying the recorded strains by the average modulus of elasticity.

For the particular test shown in Fig. 7, the stress level was so low that very little if any local buckling occurred and the beam response was essentially linear elastic. For the test in Fig. 9, however, considerable local buckling occurred and the beam response was not linear as indicated. The variation of the top flange stress at the edge of the compression flange, σ_{TOP}, and the bottom flange stress, σ_{BOT}, in Fig. 9 are smooth curves during the duration of the applied load and the response is similar to the variation of the external load pulses. The time variation for the stress at the center of the top flange, σ_{MID}, however, is irregular and is not similar to the time variation of the external load pulse. The presence of the dip in this stress trace is an indication that the top flange has buckled. Also, the reduced magnitude of stress at this point compared to the magnitude of stress at the edge of the top flange is an indication that a reduction in effective width has taken place. Note that the top flange buckled while the edge stress was increasing and recovered while this edge stress was decreasing. Records similar to those shown in Fig. 9 for other tests at higher stress levels indicated that the stress in the center of the top flange oscillated several times while the edge stress increased and decreased. These oscillations are a result of the vibrations of the individual plate elements which comprise the cross section and are superimposed on the oscillations of the overall beam vibrating as a unit.

Calculated response curves for the tests in Figs. 7, 9 obtained using the computer program and plotting routine discussed earlier are shown in Figs. 8, 10. The load pulses obtained from the oscilloscopes and the relationship between the moment and moment of inertia in the static tests were used as input to the program. Approximately fifty discrete values of the load were used at equal time intervals (0.50 milliseconds) over the duration of the positive phase of the load pulse. Since the maximum beam response, which is of primary interest, occurs in this time interval, only the positive portion of the load pulse was considered. Since the computer program replotted the input load pulse, it was possible to compare this with the oscilloscope trace in order to insure that a sufficient number of discrete points had been selected to adequately represent the experimental load pulse. Note that the added mass of the loading rings which vibrated with the beam was taken into account in these calculations.

Comparison of Figs. 7, 9 and 8, 10 indicate that the calculated maximum stresses and deflections are of the same order of magnitude as the experimental values. The calculated values were much larger than the experimental values after the load pulse was removed, however. This difference is due to the influence of structural damping and the negative portion of the load pulse which were neglected in the mathematical model. Note also that the oscillations of the stress at the middle of the compression flange in Fig. 9 are not present in Fig. 10 since the plate vibrations were not included in the mathematical model.

Additional comparisons between calculated and experimental values of the midplane maximum top flange stress, σ_{TOP}, bottom flange stress, σ_{BOT}, and midspan deflection occuring during the positive phase of the load pulse are given in Tables 1, 2. Calculated values based on the relationship between the moment and moment of inertia obtained in the static tests, the relationship using Eq. 2 and a linear elastic analysis neglecting local buckling, I/I_o = constant = 1, are given. Note that the calculated deflections obtained from the mathematical model account for the variation of the moment of inertia due to local buckling over the entire length of the beam by means of the discrete elements described previously.

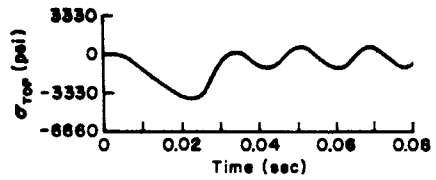

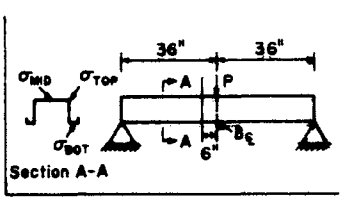

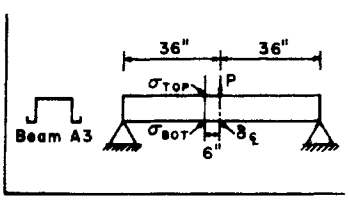

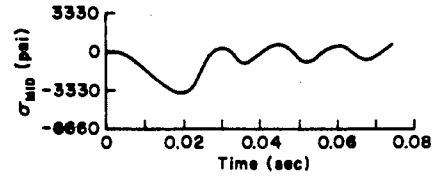

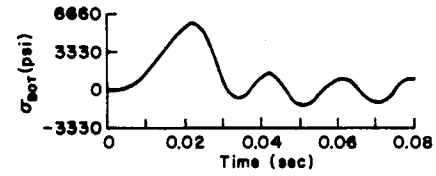

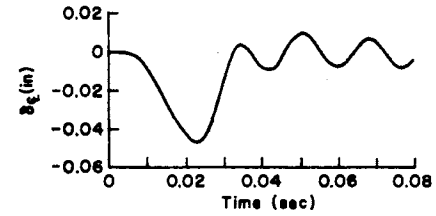

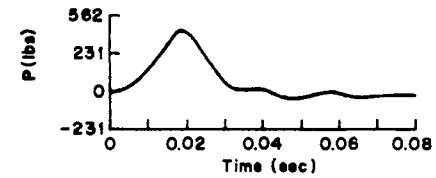

FIG. 7 - Dynamic Beam Test Traces - Specimen A - Test 1

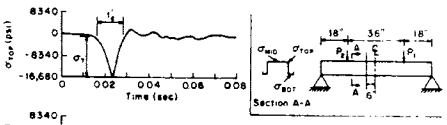

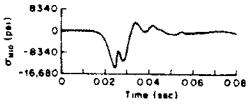

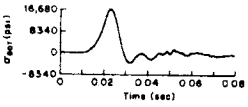

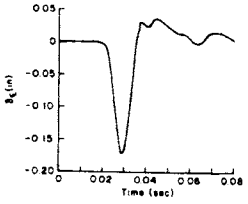

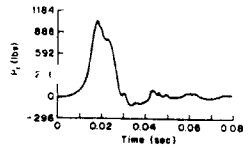

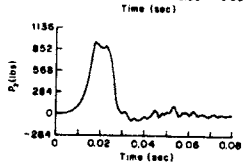

FIG. 9 - Dynamic Beam Test Traces - Specimen A - Test 13

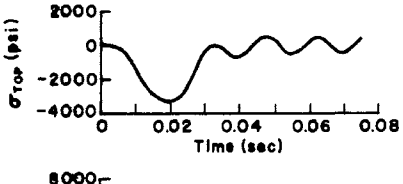

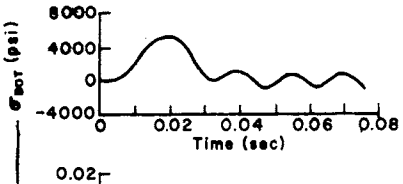

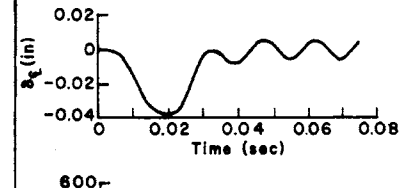

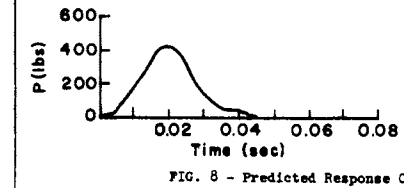

FIG. 8 - Predicted Response Curves - Specimen A - Test 1

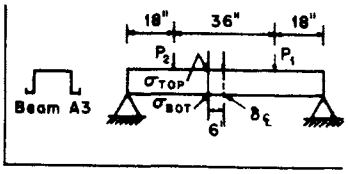

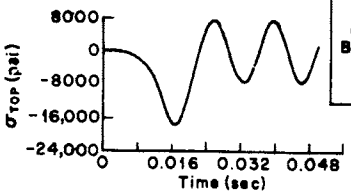

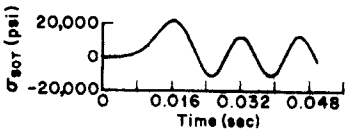

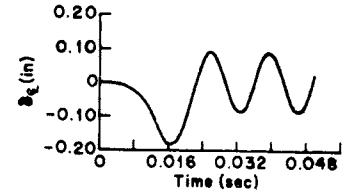

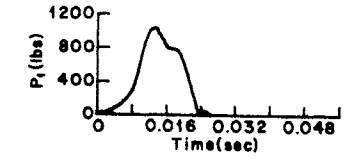

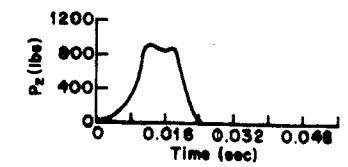

FIG. 10 - Predicted Response Curves - Specimen A - Test 13

Referring to the calculated stresses in Tables 1, 2, note that the resulting values differ for the three methods of analysis. The internal moments, not presented, obtained from the three methods, however, did not differ appreciably. Thus the method of computing the stress rather than the method used to calculate the internal moment is the more significant factor in these comparison studies. Also, the reduction in the effective width of the top flange has a greater influence on the top flange section modulus than on the bottom flange section modulus. This was indicated by the fact that in general the three methods of analysis predicted essentially the same bottom flange stress. The predicted top flange stresses, however, differed considerably.

The reduction in section modulus is influenced by the I/I_o curve. As indicated previously, the I/I_o curve based on test properties is stiffer than the I/I_o curve based on Eq. 2. Thus the analysis based on Eq. 2 generally predicted higher stresses than those predicted using the test properties. Since the internal moment predicted by all three analyses is approximately the same for a given case, the stresses in the top flange predicted by the linear elastic analysis were generally lower than those predicted using either test properties or Eq. 2. The differences between the predicted bottom flange stress and midspan deflection obtained from the three analyses were very small.

The tests in Tables 1, 2 are arranged in order of increasing stress level. The time durations of the load pulses varied between 0.0185 sec. and 0.045 sec. Note that since the stresses were within the elastic range of the material, several tests were conducted on each beam. The calculated local buckling stress based on the static tests was σ_{LB} = 6200 psi and σ_{LB} = 14000 psi for beams A3 and B4 respectively. For those tests in which the maximum top flange stress was below the value of σ_{LB}, the beam response is linear. For the tests in which the top flange stress exceeds σ_{LB}, the degree of nonlinearity is reflected by the differences between the calculated stresses based on the linear analysis and on the test properties.

For beam A3, the percentage difference between the calculated values using the static test properties and the test values for both the top and bottom flange stresses was less than 10% up to a stress level of 23,000 psi in the top flange. As the stress level increased above this value the percentage difference also increased. In general the percent difference was the same for both top and bottom flange stress. The percent difference for the deflections however, was usually larger than that for the stresses. This may have been due to experimental error since any deflection due to twisting of the beam was also recorded by the single linear differential transformer.

For beam B4 the percent difference between the values noted above was less than 10% up to a stress level of approximately 10,000 psi in the top flange. Above this stress level, the percent difference increased and was generally larger than that for beam A3. Also the percent difference was different for the top and bottom flange stress. The values in Table 2 indicate that in some cases the test values agreed more closely with those based on a linear analysis even though the beam was obviously in the postbuckling range. The poor agreement between calculated and measured values for beam B4 is due to the form of the I/I_o curve in

TABLE 1 SUMMARY OF TEST RESULTS - MIDSPAN LOADING

Beam		Test Value	Calculated Values: Test Prop.	Calculated Values: Linear Analysis	Calculated Values: Eq. 2	Difference As %: Test Prop.	Difference As %: Linear Analysis	Difference As %: Eq. 2
(1)		(2)	(3)	(4)	(5)	(6)	(7)	(8)
		(a) Top Flange Stress - σ_{TOP} (psi)						
A3	1	-3000	-2809	-2809	-2809	-7	-7	-7
	2	-3330	-3278	-3278	-3278	-2	-2	-2
	3	-3700	-3971	-3971	-3971	+5	+5	+5
	4	-6700	-6846	-6745	-7719	+2	+1	+15
	5	-8340	-9182	-8400	-10290	+10	+1	+23
	6	-9200	-9864	-8870	-10930	+7	-5	+19
B4	1	-4900	-5261	-5261	-5261	+7	+7	+7
	2	-7950	-8022	-8022	-8145	+1	+1	+2
	3	-9800	-10560	-10560	-11550	+8	+8	+18
	4	-12200	-13780	-13780	-16160	+13	+13	+32
		(b) Bottom Flange Stress - σ_{BOT} (psi)						
A3	1	3450	4432	4432	4432	+2	+2	+2
	2	5000	5172	5172	5172	+3	+3	+3
	3	5800	6266	6266	6266	+8	+8	+8
	4	10000	10570	10620	10270	+6	+6	+3
	5	11700	13170	13300	12860	+12	+14	+10
	6	12550	13860	14050	13480	+10	+12	+7
B4	1	5700	6718	6718	6718	+18	+18	+18
	2	9200	10240	10240	9728	+11	+11	+6
	3	11600	13490	13490	12970	+16	+16	+12
	4	15300	17590	17590	17050	+15	+15	+11
		(c) Midspan Deflection - δ_{ℓ} (in.)						
A3	1	0.037	0.033	0.033	0.033	-12	-12	-12
	2	0.041	0.037	0.037	0.037	-11	-11	-11
	3	0.048	0.045	0.045	0.045	-7	-7	-7
	4	0.085	0.078	0.078	0.045	-9	-9	-2
	5	0.105	0.099	0.097	0.106	-6	-8	+1
	6	0.115	0.105	0.104	0.112	-9	-10	-3
B4	1	0.060	0.059	0.059	0.059	-2	-2	-2
	2	0.085	0.089	0.089	0.090	+5	+5	+6
	3	0.115	0.118	0.118	0.123	+3	+3	+7
	4	0.138	0.154	0.154	0.166	+12	+12	+20

Difference as a percentage = $\frac{\text{Calculated - Test}}{\text{Test}}$

TABLE 2 SUMMARY OF TEST RESULTS QUARTER POINT LOADING - BEAM

Beam		Test Value	Calculated Values: Test Prop.	Calculated Values: Linear Analysis	Calculated Values: Eq. 2	Difference As a %: Test Prop.	Difference As a %: Linear Analysis	Difference As a %: Eq. 2
(1)		(2)	(3)	(4)	(5)	(6)	(7)	(8)
		(a) Top Flange Stress - σ_{TOP} (psi)						
A3	7	-2080	-2283	-2283	-2300	+10	+10	+11
	8	-5320	-5382	-5382	-6185	+1	+1	+16
	9	-5700	-6011	-6011	-7035	+5	+5	+22
	10	-10000	-9747	-8851	-11750	-3	-13	+18
	11	-12400	-11460	-9950	-13300	-8	-25	+7
	2	-14200	-14700	-11940	-16980	+4	-19	+20
	13	-16500	-17790	-13475	-20640	+8	-22	+25
	14	-22100	-23660	-16400	-26240	+7	-35	+19
	15	-22300	-24610	-16810	-27150	+10	-33	+22
	16	-23000	-27670	-18050	-30260	+20	-28	+32
	17	-26700	-32170	-19940	-33740	+20	-34	+26
	18	-28600	-35400	-21800	-37090	+24	-31	+30
	19	-32900	-40390	-24100	-41920	+22	-37	+27
B4	5	-9000	-11330	-11330	-13440	+26	+26	+49
	6	-9200	-11390	-11390	-13620	+24	+24	+48
	7	-13400	-17090	-16060	-20870	+28	+20	+56
	8	-18400	-22580	-19390	-26320	+23	+5	+43
	9	-20600	-26850	-22190	-30010	+30	+8	+51
	10	-23200	-32000	-25730	-36940	+38	+11	+59
	11	-29000	-35990	-28600	-41710	+24	-1	+44
		(b) Bottom Flange Stress - σ_{BOT} (psi)						
A3	7	3500	3602	3602	3638	+3	+3	+4
	8	7900	8492	8492	8620	+7	+7	+9
	9	9200	9485	9486	9538	+3	+3	+4
	10	13750	13740	13970	14260	0	+2	+4
	11	15400	15390	15700	15720	0	+2	+2
	12	17500	18300	18840	19050	+5	+8	+9
	13	17600	21100	21260	22240	+20	+21	+26
	14	23000	25630	25580	26900	+12	+13	+17
	15	22300	26290	26530	27660	+18	+19	+24
	16	24200	28400	28480	30160	+17	+18	+25
	17	25000	31310	31470	32940	+25	+26	+32
	18	27500	33680	34400	35550	+23	+25	+30
	19	28300	37840	38030	39280	+34	+34	+39
B4	5	11000	14470	14470	14680	+31	+31	+34
	6	11500	14550	14550	14830	+26	+26	+29
	7	15300	20140	20500	21020	+32	+34	+37
	8	19100	24070	24760	25420	+26	+29	+33
	9	20900	27650	28340	29100	+33	+36	+40
	10	23400	23440	32060	33650	+39	+37	+44
	11	29500	36420	36500	37220	+23	+24	+26
		(c) Midspan Deflection* - δ_{ℓ} (in.)						
A3	7	0.035	0.030	0.030	0.030	-17	-17	-17
	8	0.075	0.070	0.070	0.072	-7	-7	-4
	9	0.081	0.077	0.076	0.080	-7	-6	-1
	10	0.115	0.116	0.114	0.126	+1	-1	+10
	11	0.125	0.133	0.125	0.136	+4	0	+9
	12	0.145	0.165	0.156	0.179	+14	+7	+23
	13	0.175	0.186	0.170	0.204	+6	-3	+16

*Deflection data not obtained for Tests 14 thru 19

the nonlinear range. Beam B4 was considerably stiffer than beam A3 and the slope of the I/I_o curve in the postbuckling range for B4 was much steeper than that for A3 (Fig. 5). The stiffness of beam B4, therefore, was considerably more sensitive than beam A3 to slight changes in the internal moment. At the higher stress levels, agreement between calculated and measured values were similar for both beams.

The percent difference between the calculated values using Eq. 2 and the test values was larger than that obtained using the static test values due to the differences between the moment versus moment of inertia relationship mentioned previously (Fig. 5).

A presentation of all the static and dynamic test results obtained in this investigation is given in Fig. 11. The form of this graph is the same as that used by Winter (11) in establishing existing requirements for calculating effective width. Reduction of the static test data for this graph was the same as that used by Winter. For the dynamic tests, calculation of the effective width b, and σ_T in Fig. 11 were based on the maximum midplane top flange stress which occurred during the positive phase of the load pulse. The dynamic test points therefore represent the minimum effective width which occurred during each test. The values of the abscissa above which the full width of the compression flange is effective and also the values for which the maximum top flange stress is less than the yield stress are also shown.

As noted previously, earlier studies (2) indicated that the effective width in a dynamic test would be influenced by the vibration of the plate elements comprising the cross section. In order to determine whether any trend existed, the dynamic data in Fig. 11 was grouped according to the value of β' or the ratio of the time duration of the stress pulse (Fig. 9) to the fundamental period of the compression flange treated as a simply supported plate. The dynamic test results in Fig. 11 do not indicate any such trend. The scatter of the dynamic data is similar to that in the static tests. Also, with the exception of a few of the dynamic tests for beam A3 at high stress levels, the relationship in Eq. 2 fits both the static and dynamic results to the same degree of accuracy obtained in earlier studies (11). Based on these results, the use of Eq. 2 for calculating the moment versus moment of inertia relationship to be used for dynamic response calculations of thin-walled beams subjected to impact loading appears justified.

In discussing the calculated values presented in Tables 1, 2, it was noted that although the stresses and deflections obtained by the three methods differ substantially when the beam is in the postbuckling range, the internal moments, however, did not differ appreciably. This fact suggests that for design purposes, it may be possible to forego the complicated incremental type solution of the equations of motion presented herein and simply use the as built section properties of the beam and well established linear elastic response techniques such as normal mode superposition, etc. to determine the internal moments produced by the impact loads. Using these moments and the appropriate reduced section properties based on Eq. 2, the internal stresses and deflections could then be calculated in the same manner as is presently used for cold-formed beams subjected to static loads. The adequacy of this technique for design purposes as well as the influence of the various nondimensional parameters on the dynamic response will be considered in a forthcoming paper based on completed studies (8).

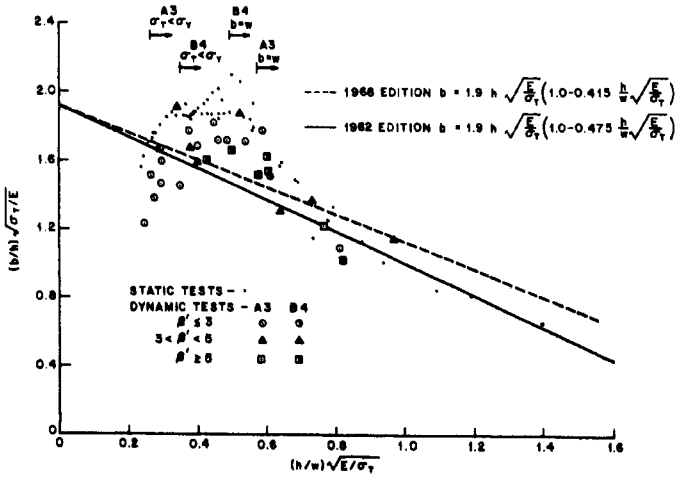

FIG. 11 - Static and Dynamic Test Results

SUMMARY AND CONCLUSIONS

The behavior of thin-walled, cold-formed beams subjected to impact loading was studied both analytically and experimentally. The experimental study consisted of static and dynamic tests. The results of this investigation indicated that in order to determine the stresses and deflections of thin walled beams subjected to impact, it is necessary to take into account the postbuckling behavior and include the concept of effective width. The use of existing expressions for this effective width which are based on static test results appear adequate for calculating the dynamic response. Preliminary calculations indicate that it may be possible to use linear elastic response techniques to determine the internal forces in structures of this type.

ACKNOWLEDGMENTS

The results presented herein were taken from a doctoral thesis submitted by Edward A. Zanoni to the Department of Civil Engineering, Carnegie-Mellon University. Charles G. Culver served as the thesis advisor. This work represents the second phase of a research program on "Light Gage Cold-Formed Structural Elements Subjected to Time-Dependent Loading" sponsored by the American Iron and Steel Institute at Carnegie-Mellon University. The cooperation of W. G. Kirkland, Vice President, AISI, and the members of the AISI Task Group on the Influence of Dynamic Loading on Structural Behavior of Light Gage Steel, R. B. Matlock, Chairman, J. B. Scalzi and C. R. Clauer is gratefully acknowledged.

APPENDIX I - REFERENCES

1. Argyris, J., and Kelsey, S., Energy Theorems and Structural Analysis, Butterworth and Co. Ltd., London, 1960.

2. Culver, C., Van Tassel, R., "Shock Loading of Thin Compression Elements,"

3. Johnson, A. L, Winter, G., "Behavior of Stainless Steel Columns and Beams," Journal of the Structural Division, ASCE, Vol 92, No ST5, Proc. Paper 4934, October, 1966, pp 97-118.

4. Light Gage Cold-Formed Steel Design Manual, American Iron and Steel Institute, New York, 1962.

5. Newmark, N., "A Method of Computation for Structural Dynamics, Transactions ASCE, Vol 127, 1962, Part I, p 1406.

6. Newmark, N., Walker, W., Veletsos, A., and Mosberg, R., "Design Procedures for Shock Isolation Systems of Underground Protective Structures," Newmark, Hansen and Associates, Urbana, Illinois, Technical Report No. RTD TDR 63-3096, Vol IV, December, 1965.

7. O'Hara, G., "Shock Spectra and Design Shock Spectra, Naval Research Laboratory, Report 5386, November, 1959.

8. Osgood, A., "Response Spectra for Light Gage Cold-Formed Beams," Thesis submitted to Carnegie-Mellon University, Pittsburgh, Pennsylvania, 1969, in partial fulfillment of the requirements for the degree of Master of Science.

9. Specification for the Design of Cold-Formed Steel Structural Members, American Iron and Steel Institute, New York, N. Y., 1968.

10. Wilson, E., and Clough, R., "Dynamic Response by Step-by-Step Matrix Analysis," Symposium on the Use of Computers in Civil Engineering, National Laboratory of Civil Engineering, Lisbon, Portugal, Paper No. 45, October 1962.

11. Winter, G., "Performance of Thin Steel Compression Flanges," Cornell University Eng. Exp. Sta., Reprint No 33, November, 1950.

12. Yu, W. W., "Design of Light Gage Cold-Formed Steel Structures," Engineering Experiment Station, West Virginia University, 1965.

13. Zanoni, E. A., "Nonlinear Analysis of Light Gage Cold-Formed Beams Subjected to Shock Loading," University Microfilms, Ann Arbor, Mich., 1969.

APPENDIX II - NOTATION

The following symbols are used in this paper:

a_i = time coefficient at load point;

a_i' = nondimensional time coefficient at load point;

a_{11}, a_{12} = flexibility coefficient;

b = effective width of top flange of beam;

b_i = nondimensional mass coefficient for mass point i;

c = distance from the neutral axis to extreme top flange fiber of beam;

c_o = c computed from the original cross section properties;

E = modulus of elasticity;

e = subscript used to denote element;

f = flat width of bottom flange of beam;

h = thickness of beam element;

I = moment of inertia;

I_o = I computed from the original cross section properties;

i = mass point designation;

j = number of beam elements;

L = span length of beam;

l = length of beam element;

M = total mass of beam;

M_c = characteristic moment;

M_e = moment at element location e;

M_{LB} = local buckling moment

m_i = magnitude of lumped mass at point i;

P_i = magnitude of applied load at point i;

P_m = characteristic load magnitude;

Q_i = net internal force at point i;

S_B = section modulus for bottom flange of beam;

S_{BO} = section modulus for bottom flange of beam computed from original cross sectional properties;

S_T = section modulus for top flange of beam;

S_{TO} = section modulus for top flange of beam computed from original cross sectional properties;

S_o = initial imperfection parameter - Fig. 3;

t = time;

t_d = time duration of load pulse;

t_d' = time duration of stress pulse;

t_o = fundamental natural period of beam;

V_e = shear at element location e;

w = flat width of top flange of beam;

x_i = nondimensional displacement of mass point i;

$\ddot{x}_i$ = nondimensional acceleration of mass point i;

y_i = absolute displacement of mass point i;

$\ddot{y}_i$ = absolute acceleration of mass point i;

α = nondimensional beam loading;

β = nondimensional load duration for beam response;

β' = nondimensional load duration for plate response;

δ_ℓ = midspan deflection;

δ_P = characteristic deflection;

ϵ = strain;

ϵ_{DYN} = maximum dynamic strain in plate;

ϵ_{Static} = maximum static strain in plate;

η = characteristic deflection coefficient;

λ = nondimensional length coefficient;

ξ = coefficient for characteristic moment;

$\bar{\sigma}$ = maximum edge stress;

σ_B = maximum bottom flange stress in beam;

σ_{CR} = critical stress for restrained plate element;

σ_{LB} = local buckling stress for beam;

σ_T = maximum top flange beam stress;

σ_y = yield stress;

τ = nondimensional time

Matrix Notation

$\left[\ \right]$ = matrix;

$\left[\ \right]$ (diagonal) = diagonal matrix;

$\left[\ \right]^T$ = transposed matrix;

$\left[\ \right]^{-1}$ = inverted matrix;

$\{\ \}$ = column vector;

Specially Defined Matrices

$\left[A\right]_B$ = beam flexibility matrix;

$\left[A\right]_e$ = element flexibility matrix;

$\left[C\right]_e$ = element connection matrix for shear and moment;

$\left[CR\right]_e$ = nondimensional element connection matrix for moment;

$\left[F\right]_B$ = nondimensional beam flexibility matrix;

$\left[I\right]$ = identity matrix